

A Systematic Global Mapping of the Radiation Field at Aviation Altitudes

E. G. Stassinopoulos, C. A. Stauffer, G. J. Brucker

Abstract-- This paper presents early results from aircraft measurements made by a Low-LET Radiation Spectrometer (LoLRS), as part of a long-range effort to study the complex dynamics of the atmospheric radiation field. For this purpose, a comprehensive data base is being generated to enable a multivariable global mapping (and eventually modeling) of doses and Linear-Energy-Transfer (LET) spectra at aviation altitudes. To accomplish this, a methodical collection of data from the LoLRS (and other instruments), is planned over extended periods of time, in a manner that complements some previous isolated and sporadic measurements by other workers, with the objective to generate a detailed long-range description of the cosmic-ray induced particle environment and to study its variability and dependence on atmospheric thickness, magnetic latitude, L-shell or rigidity, space weather, solar particle events, solar cycle effects, magnetic field variation, diurnal and seasonal effects, and atmospheric weather. Analysis of initial data indicates that the dose is rising with increasing altitude and increasing magnetic latitude. Comparison of total doses with predictions is in good agreement.

I. BACKGROUND

The introduction in recent years of new "fly-by-wire" aircraft, as for example the Boeing-777, the European Airbus, and the high altitude supersonic Concorde (16-18 km), has raised some serious concerns about the safety and reliability of their operation in the intense cosmic-ray produced radiation field of neutrons, protons, and other particles in the earth's atmosphere, Figure 1 [1]. Single Event Effects (SEE) vulnerability of on-board computers that regulate the navigational, flight control, communication, and life support systems has become an issue in advanced, modern aircraft [2,3,4,5]. The next generation of such aircraft are most likely going to use new technologies that will be far more sensitive than anything used before, technologies such as 0.25 μm feature size devices with 64 to 124 megabit integration levels, operating with biases of less than 2.5 volts, and with multi-terabit memory banks. This substantially increases the need to

improve the definition of the atmospheric radiation field as a function of location and time, and to reduce the significant uncertainties associated with present day predictions.

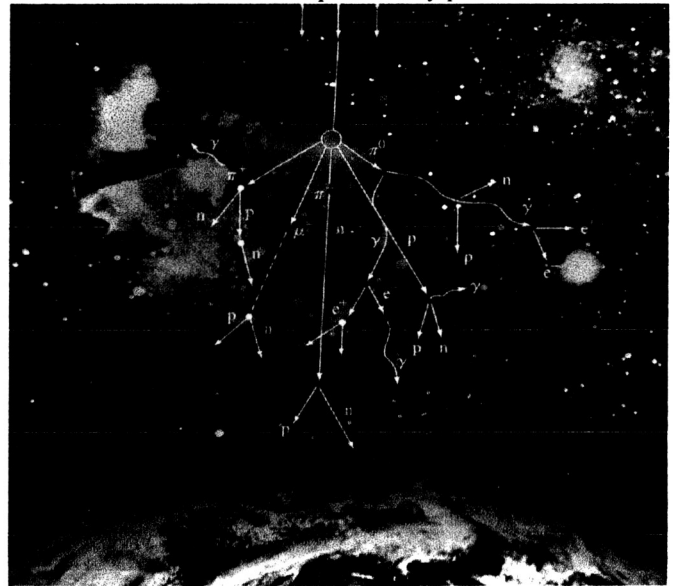


Figure 1: Cosmic Ray Daughter Products in the Earth's Atmosphere (Courtesy IBM). [1]

To address these concerns, dual-purpose novel state-of-the-art radiation monitors/spectrometers have been developed to measure the energy deposited in their detectors by the cosmic rays and their progeny [6,7] in order to obtain LET spectra (in units of $\text{keV}/\mu\text{m}$) for SEE evaluations in electronic systems, and to obtain total dose and dose rate values for assessing health hazards to crews and passengers. The LoLRS instrument, primarily used in this effort, is a low power, small size, light weight radiometer capable of measuring heavy particle distributions having LET values in the range of 0.591 to 13.8 $\text{keV}/\mu\text{m}$ (Si). The detector is a Silicon-Lithium Drifted Diode, 1 mm thick, with a sensitive area of 1 cm^2 and weight of 0.232g. A detailed description of the instrument is given in Reference [7].

Although a number of uncorrelated studies have been done before to define the atmospheric radiation environment and to learn to predict its impact on aviation, this is the first effort to systematically investigate the premise that several major physical processes may significantly affect the distribution and intensities of the atmospheric radiation levels over short – and long-term scales and to quantify the effect of these processes.

E. G. Stassinopoulos is with NASA Goddard Space Flight Center, Greenbelt, Maryland, 20771 USA (telephone: 301-286-8594, e-mail: Epaminondas.G.Stassinopoulos@nasa.gov).

C. A. Stauffer is with Stinger Ghaffarian Technologies, Greenbelt, Maryland 20771 USA (telephone: 301-286-4011, e-mail: Craig.A.Stauffer.1@gssc.nasa.gov).

G. J. Brucker is with the Radiation Effects Consultants, Inc., West Long Branch, NJ 07764 USA

Thus, several experiments have been performed in the past by other workers [2-5, 8-12], however, the extent of these measurements has been limited in scope and duration, and does not provide the long term, continuous coverage necessary to address global conditions and establish a history of slow-variation effects.

In the initial phase of the present investigation, EVERGREEN International Airlines, a commercial cargo carrier, has rendered, as an active research partner, valuable assistance by flying the LoLRS on their Boeing 747 cargo planes for continuous and repetitive flights over their extended routes, which in time will enable us to study the long-term effects of solar and environmental influences on the radiation field in the atmosphere at aviation altitudes. The flight paths available for data collection are displayed in Figure 2. Lately, polar crossings have been added to these routes.

The purpose of this paper is to describe the methodology and present an example of the mapping program with some preliminary results. The ultimate objective is to eventually define the dependence of radiation exposure at aviation altitudes in terms of: 1. atmospheric thickness, 2. magnetic latitude (or equivalently: magnetic L-shell or Rigidity), 3. space weather, 4. solar particle events, 5. solar cycle, 6. magnetic field variability, 7. diurnal and seasonal variations, and 8. atmospheric weather. This goal presupposes: a. that measurements extend over long periods of time (years), and b. the accumulation of large amounts of data in order for the results to be statistically significant.

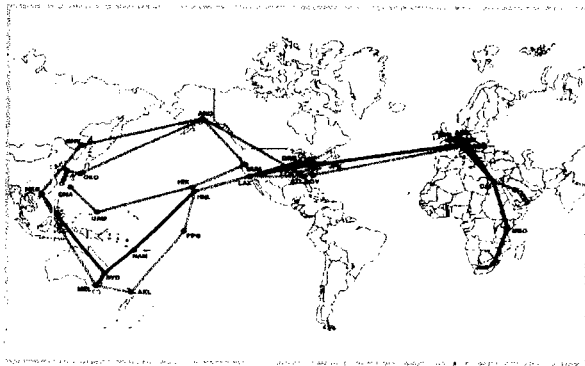


Figure 2: Frequently Traveled Routes of 747 Cargo Planes

II. MAGNETOSPHERIC SHIELDING, RIGIDITY, AND L. SHELL PARAMETER

The magnetic shell parameter L [13] is defined as the geocentric distance to the equatorial crossing of the field line passing through the position at which the measurement was made.

The effect of the earth's magnetic field to deflect incoming galactic and solar cosmic rays is expressed as rigidity R in units of GV and is given in terms of particle momentum-over-charge by:

$$R = (1/q)(E^2 + 2mE)^{0.5} \quad (1)$$

where m is particle mass, E is its energy, and q is its charge. Conversion of R to the magnetic shell parameter L is achieved through the relationship:

$$L = (14.9 / R_c * 10^{-3})^{0.5} \quad (2)$$

where here R_c is the vertical rigidity cutoff in units of MV. Values of R_c have been published in [14] and further described in [15].

This concept is graphically depicted in Figure 3 [16], where field lines of L from 2 to 7 are plotted, intersecting the earth at corresponding magnetic latitudes. The energies required to penetrate up to each of these field lines (the cutoff energies E_c) are listed for hydrogen in the upper half and for heavier ions in the lower half of the drawing. The intersects of the field lines on the surface of the earth (or at any given altitude level), trace out the L -shell isocontours projected onto the world map (see Figure 8).

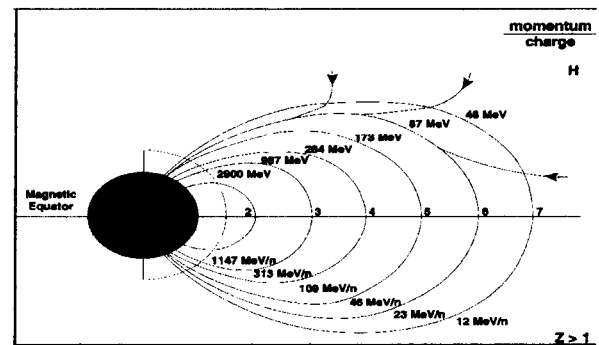


Figure 3: Total Energy Required to Penetrate the Earth's Magnetic Field (Magnetic Rigidity) [16].

III. ATMOSPHERIC NEUTRON MODELS

Existing atmospheric neutron models are the earliest practical application-oriented tools designed by two groups of scientists approaching this topic from different directions with different motivations. One model was attempted by Taber and Normand [17]. It was based on measurements from several sources [18,19,20] and it was used by Normand and Baker to calculate Single Event Upset (SEU) rates at aircraft altitudes [15]. It was not very accurate and it did not reflect well the energy distribution of the neutrons. The other attempt was an improved model constructed by Wilson and Nealy [21]. It had greater accuracy in the 1-10 MeV energy range, with the added advantage that it did account for neutron variations with solar activity, but only on the basis of relative measurements from ground-station neutron monitors. It was intended primarily for radiobiological studies. Neither model addressed environment induced variations.

IV. POLAR MEASUREMENTS OF COSMIC RAY PROGENY

Of special interest are the areas over the polar regions, where open field lines connect directly to interplanetary space and cosmic rays do not experience magnetospheric

attenuation; that is, these areas are freely accessible to all energies of heavy ion spectra, while only a few very energetic particles (GeV/n) can penetrate to the equatorial regions. The abundance of cosmic ray progeny is consequently at a minimum near the equator and at a maximum near the poles. Of course, ion penetration depends also to a large degree on their level of ionization. For galactic cosmic rays it is assumed that they arrive at the vicinity of our planet fully ionized. The arrows in Figure 3 are an example, showing the limit of penetration of 87 MeV hydrogen atoms up to an L-shell crossing the magnetic equator at 6 earth radii.

Cosmic rays and their secondary neutrons (in addition to other particles produced by them in the atmosphere or in aircraft materials) are an important, and sometimes dominant, component of the radiation environment at high aircraft altitudes for instruments, electronic circuits, and crews and passengers. Measurements of these particles over the polar regions are especially important because they may serve as a standard by which to gauge the effect of magnetospheric shielding at other locations on the globe, thus allowing a true definition of rigidity in terms of cut-off latitudes, solar cycle effects, and space weather conditions. The results can then be used to improve existing models [17,21] or construct a new empirical model, reflecting to some degree the dynamic nature of the atmospheric neutron environment and reduce uncertainties in predictions. High-altitude (up to 39 km), long-duration balloon flights (weeks to months) over Antarctica are ideal to obtain the best measurements that will provide this standard. Balloon experiments of this type have been successfully tested and are being planned for the future.

V. VARIABILITIES, DEPENDENCIES, AND UNCERTAINTIES

The number of primary cosmic rays reaching any region in the Earth's atmosphere, and hence the number of the corresponding daughter products present, is controlled by the defining parameters R_c and E_c . However, the values of R_c and E_c , associated with a given geographic location, are not constant but experience short-term and long term variations.

Long-term variations are primarily the effects of slow changes induced by the secular variation of the Earth's magnetic field (gradually decreasing in strength), the drift of the magnetic poles, and the solar cycle modulation of the cosmic ray fluxes.

Short-term variations include diurnal and seasonal effects, the effects from space weather (as for example: solar wind, magnetic storms, etc.), solar particle events (flares, coronal mass ejections {CMEs}), and atmospheric weather conditions.

Storm induced magnetic variability, usually expressed by the K_p and D_{st} indexes, affects the atmospheric radiation levels because it rapidly changes the local values of the associated critical parameters E_c and R_c (or the equivalent L-shell values) that define these fluxes at any given position on the globe. This results in storm-time suppression of geomagnetic cutoff which leads to increase in exposure.

Ground level event (GLE) measurements are also affected by these variabilities.

Regarding the secular variation of the Earth's magnetic field, it is important to establish its impact on the atmospheric cosmic-ray progeny levels (we assume non-uniformity over a global scale) and to quantify its effects on positional measurements as a function of time, for similar environment conditions. Data obtained many years ago can then be adjusted and combined with later measurements, to be used in correlations, or incorporated in global mappings, or included in modeling processes.

Another issue to be considered is to ascertain if and to what extent the cosmic-ray primary and secondary radiation intensities are being modified by: 1. atmospheric thickness, 2. material shielding of carrier, payloads, and enclosures, 3. subtended Earth exclusion angle, 4. north-south asymmetry, and 5. east-west asymmetry.

In all cases, the intrinsic errors in collecting and processing data, interpreting the measurements, and reaching conclusions, need to be determined in order to establish the degree of uncertainty associated with the final results, models, or predictions.

VI. OBJECTIVES

The primary aim of continually flying radiation spectrometers on a multitude of carriers (aircraft, unpiloted aviation vehicles, balloons, etc.) over long periods of time is to accumulate sufficient information that will broaden our understanding of the very dynamic nature of the atmospheric radiation environment regarding composition, spectral distribution, intensity, and temporal and spatial variations. In that way it will be possible to improve the reliability of predictions and to reduce the uncertainties associated with estimates of crew exposure and safety of electronics.

VII. METHODOLOGY

The data accumulated in 5-minute collection intervals from the various campaigns and flight schedules in the initial phase of this study were compiled into a single "master" database of time- and position-tagged measurements, to which critical parameters are being added, describing the conditions prevailing at the location and the time at which the data were collected, as for example: magnetic parameters (field strength B , magnetic shell value L , rigidity R), cut-off energy E_c , local time LT , season of year, place in solar cycle, space weather conditions (magnetic storms, solar wind intensity, K_p index), and atmospheric weather conditions.

For the purpose of this paper, the available data were processed and analyzed in terms of only those variables and parameters that could be evaluated at this time. Long-range effects will be investigated much later when adequate measurements have been collected to allow such an analysis. For now, the data were sorted into 5 groups of 49 channels each. As most of the measurements were concentrated in

groups 1 and 2, these were further divided into 7 subgroups of 7 channels each. The corresponding energy and LET ranges are given in Table 1, in units of MeV and keV/ μm , respectively. The values of both quantities are equal because of the 1 mm depth of the detector: $1 \text{ keV}/\mu\text{m} = 1$

MeV/mm = $4.255 \text{ MeV}\cdot\text{cm}^2/\text{g}$ for amorphous silicon density of $2.35 \text{ g}/\text{cm}^3$. The last channel (#256) is integrating all events that deposited energies greater than 13.750 MeV. A schematic representation of this arrangement is shown in Figure 4, including the breakdown of group 1 into subgroups. The data from eight initial flights, obtained during quiet solar maximum conditions, were then ordered according to magnetic shell parameter L and altitude (in ft) to produce Table 2.

TABLE I
ENERGY RANGES (GROUPS/SUBGROUPS)

MeV	Grp	MeV	Subgrp
0.591 - 3.223	1	0.591 - 0.967	1a
3.223 - 5.854	2	0.967 - 1.343	1b
5.854 - 8.486	3	1.343 - 1.719	1c
8.468 - 11.118	4	1.719 - 2.095	1d
11.118 - 13.750+	5	2.095 - 2.471	1e
		2.471 - 2.847	1f
		2.847 - 3.223	1g

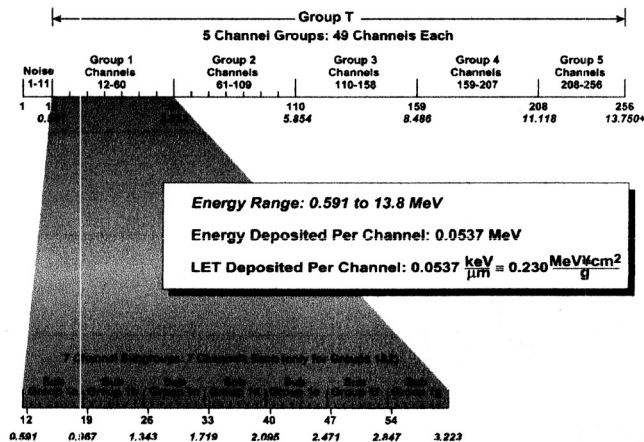


Figure 4: Channel Groupings and Deposited Energy Ranges for 256 Channels

VIII DOSE CALCULATIONS

The major parameter of the instrument is the amplitude of the charge pulses generated in the solid state detector by the incident particles. The pulses are passed to the charge-sensitive amplifier that converts them to corresponding voltage pulses. The sensitivity or conversion factor of this amplifier is 240 mV/MeV. Since there are 256 channels in the Analog-to-Digital converter and the upper voltage limit is 3.3 V, the sensitivity per channel is $3.3/256=12.89 \text{ mV}/\text{ch}$, or equivalently $0.05371 \text{ MeV}/\text{ch}$, as obtained from the ratio of $12.89 \text{ mV}/\text{ch}$ to the AMPTEK charge sensitive amplifier

sensitivity of 240 mV/MeV. Since the first eleven channels were assigned to instrument noise, the effective energy threshold of the instrument is that of the 12th channel, namely 0.591 MeV. The deposited energy E_d (MeV) in channels 12 to 256 is given by the equation:

$$E_d (\text{MeV}) = 0.05371 (\text{MeV}/\text{ch}) * \sum_{ch=12}^{256} (\text{counts}_{ch} * \text{ch}) \quad (3)$$

and the dose is given by:

$$D(\text{Gy}) = \text{Joules} / M \quad (4)$$

where M is the mass of the detector in kilogram. As the volume of the detector is 0.1 cm^3 and the silicon density is $2.35 \text{ g}/\text{cm}^3$, the mass of the detector amounts to $2.35 \times 10^{-4} \text{ kg}$. The conversion of energy to Joules is obtained from:

$$\text{Joules} = E_d (\text{MeV}) * 1.6021917 \text{ e}^{-13} (\text{Joules} / \text{MeV}) \quad (5)$$

Substituting (5) into (4) yields the total dose measured in units of Gray. The respective dose rate can be obtained from:

$$D_r (\mu\text{Gy} / \text{sec}) = 1 \times 10^6 (\mu\text{Gy} / \text{Gy}) * D(\text{Gy}) / t_m \quad (6)$$

where t_m is the measurement time in seconds.

IX RESULTS

An example of the LoLRS measurements of dose rate versus time for a flight from Anchorage to Hong Kong is shown in Figure 5. The rate data are plotted separately for groups 1, 2 and for all groups, that is, for the total energy range. A similar plot of dose rate data for the same flight is displayed in Figure 6 but now the subgroups 1a, 1b, and 1c, are compared to the total of group 1 for the energy range of 0.591 to 3.223 MeV. Another method for examining the response of the instrument is illustrated in Figure 7, where the differential spectra for two intervals of time (flight segments of one hour each) during the same Anchorage to Hong Kong flight are shown. The Anchorage and Melbourne to Hong Kong flight paths are shown superimposed on a map of geographic latitude versus longitude in Figure 8, where constant L-shell contours are also plotted.

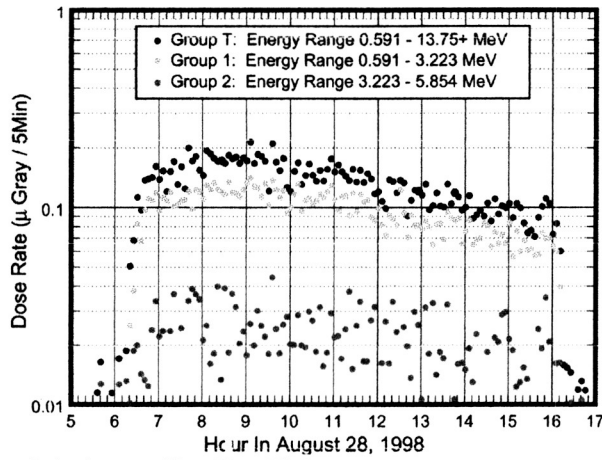


Figure 5: Anchorage - Hong Kong Flight

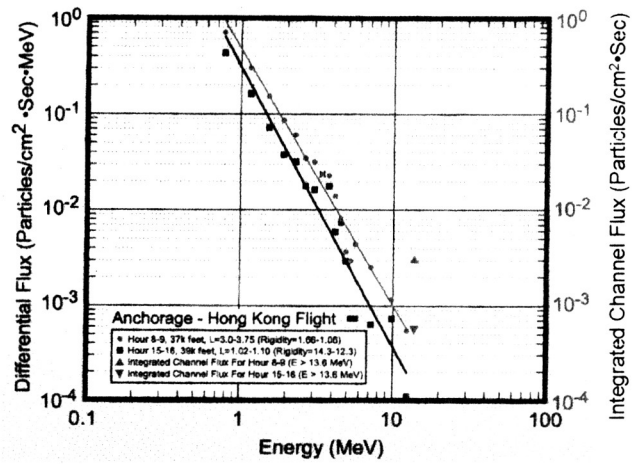


Figure 7: Differential Spectra for two selected time intervals from the Anchorage to Hong Kong flight.

TABLE II
PRELIMINARY RESULTS BASED ON 8 FLIGHT SEGMENTS ONLY

Alt. Bin

(Values In [] Indicate the Number of Measurements)

11.9 km	8.88 E-2 [35]	9.43 E-2 [18]	8.93 E-2 [12]	9.77 E-2 [9]	1.03 E-1 [9]	1.11 E-1 [5]	1.16 E-1 [6]	1.22 E-1 [7]	1.27 E-1 [5]	1.79 E-1 [2]	1.85 E-1 [2]	1.87 E-1 [1]	1.85 E-1 [3]	1.78 E-1 [2]	2.03 E-1 [3]	1.96 E-1 [2]	2.12 E-1 [3]	2.08 E-1 [5]	1.94 E-1 [6]	2.00 E-1 [5]	2.01 E-1 [17]	1.94 E-1 [3]	
11.3 km		7.94 E-2 [6]						1.90 E-1 [2]	2.05 E-1 [3]	1.41 E-1 [3]	1.46 E-1 [3]	1.61 E-1 [4]	1.46 E-1 [5]	1.53 E-1 [5]	1.49 E-1 [5]	1.71 E-1 [4]	1.89 E-1 [3]	1.75 E-1 [8]	1.73 E-1 [7]	1.86 E-1 [2]			
10.7 km		8.38 E-2 [13]	9.51 E-2 [14]	1.33 E-1 [13]	1.40 E-1 [13]	1.37 E-1 [11]	1.41 E-1 [6]	1.42 E-1 [4]	1.49 E-1 [3]													1.47 E-1 [4]	
10.1 km		6.91 E-2 [6]	7.08 E-2 [18]	7.11 E-2 [14]	7.11 E-2 [11]	7.73 E-2 [11]	8.82 E-2 [15]	8.22 E-2 [6]	8.62 E-2 [2]													1.43 E-1 [8]	
9.4 km		7.18 E-2 [30]	6.26 E-2 [5]	7.67 E-2 [15]	8.64 E-2 [10]	9.15 E-2 [8]	9.14 E-2 [2]																
8.8 km			6.21 E-2 [1]																				
	0.85 (20.8)	0.95 (16.5)	1.05 (13.5)	1.15 (11.3)	1.25 (9.5)	1.35 (8.2)	1.45 (7.1)	1.55 (6.2)	1.65 (5.5)	1.75 (4.9)	1.85 (4.4)	1.95 (3.9)	2.10 (3.4)	2.30 (2.8)	2.50 (2.4)	2.70 (2.0)	2.90 (1.8)	3.25 (1.4)	3.75 (1.1)	4.25 (0.8)	4.75 (0.7)	5.25 (0.5)	

L-Shell Bin (Ridigity Bin)

Normalized Total Doses in µ Gray / 5min

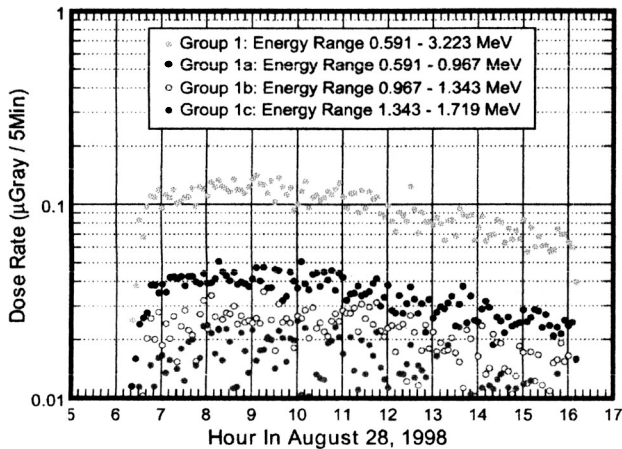


Figure 6: Anchorage - Hong Kong Flight

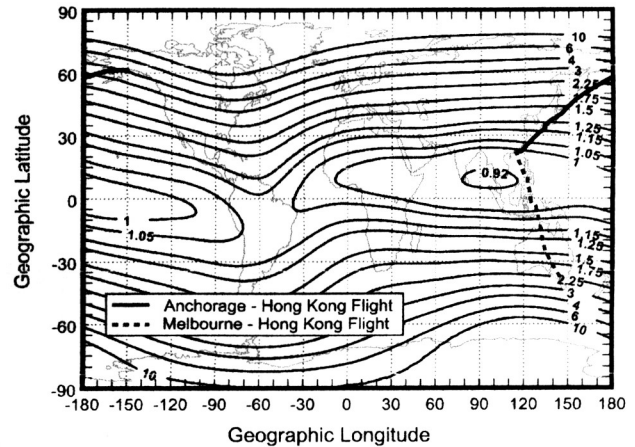


Figure 8: L-Shells at 10 km Aircraft Altitude

X. DISCUSSION

The major flight paths of the planes carrying the LoLRS instruments are shown in Figure 2. The routes provide a nearly global coverage by visiting regions from equatorial to sub-polar magnetic latitudes over a wide range of longitudes, which satisfy the goals of this investigation by repeatedly covering the same flight paths for long periods of time, whereby effects from solar, space weather, or magnetic events may be studied. The recent addition of occasional flights over the poles expanded the acquisition of measurements to a most desirable area.

Figure 4 displays a breakdown of the instrument's 256 channels into five groups. The first eleven channels are allocated to storing low level noise pulses and the remaining channels 12 to 256 make up the five groups. Each of the first two groups is further subdivided into seven subgroups of seven channels each. This process is illustrated in Figure 4 for the first group. By grouping the data in that way and then plotting dose rates versus time of flight for selected groupings, provides information on the energy distributions of incident particles. Figure 5 shows that particle energies in the range of 0.591 to 3.223 MeV (group 1) dominate the dose rate for the Anchorage to Hong Kong flight and Figure 6 indicates that the major contributor to this group is the subgroup 1a in the energy range of 0.591 to 0.967 MeV.

The differential spectra plots in Figure 7, covering two intervals of flight periods between hours 08:00 to 09:00 (at 11.3 km {37000 ft}) and 15 to 16 (at 11.9 km {39000 ft}) of the Anchorage-Hong Kong route, display how rapidly the particle fluxes decrease with increasing energy and how strongly the radiation intensity varies with magnetic latitude. The corresponding L-shells for these intervals were equal to mean values of 3.4 (high magnetic latitude) and 1.06 (low magnetic latitude), respectively, and although the altitude of period 8 to 9 was lower than that of period 15 to 16, the flux amplitudes were larger because of the higher L-values, as would be expected.

The instrument was designed with a special feature allowing it to record all particles with LET greater than 13.75 keV/ μ m and accumulate their counts in the integrating channel #256. These integral fluxes for the two flight-segments on the Anchorage-Hong Kong trip are presented in Table 3. They yield the values of 3×10^{-3} particles/cm²-s for the first segment and 5.5×10^{-4} particles/cm²-s for the second segment. Two important facts emerge from these data: a) that the integral flux for period 8-9 is greater than that of period 15-16 by a factor as large as 6 in spite of its lower altitude, which indicates a much stronger latitude dependence than anticipated on the basis of rigidity considerations alone, and b) that for both periods the integral flux for energies $E > 13.75$ MeV is large, implying a possible hardening of the spectra in the 14-100 MeV range. This, however, cannot be resolved due to the limitations of the instrument.

Flight

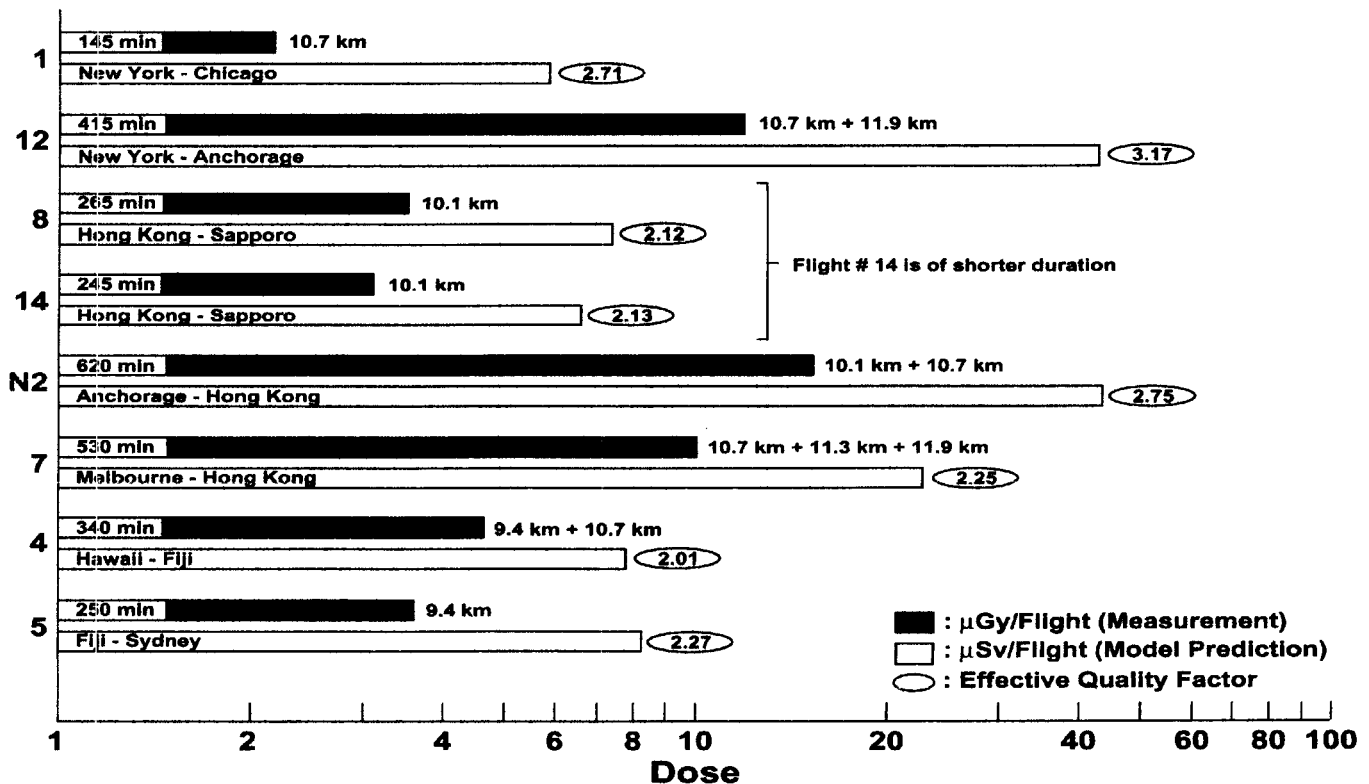


Figure 9: Comparison of Flight Measurements to Predictions (Aviation Radiation Exposure Model CARI-5E, Civil Aeromedical Institute, FAA)

TABLE III
FLUX ACCUMULATION IN INTEGRATING CHANNEL 256 FOR
ANCHORAGE-HONG KONG FLIGHT

GMT Time Interval (from hr-to-hr)	Flight Altitude (km)	Mean L-Shell Value	Flux in Channel 256 (#/cm ² •s)
8 - 9	11.3	3.4	3.0×10^{-3}
15 - 16	11.9	1.06	5.5×10^{-4}

Figure 8 is a plot of L-shell isocontours at a 10 km altitude level. The L values were calculated with the International Geophysical Reference Field (IGRF) of epoch 1995, projected to the year 1998 with its secular variation time derivatives, including contributions of the external field sources from the Tsyganenko 1996 model [22]. Indicated are traces of two flights to Hong Kong, one from Melbourne, Australia, and one from Anchorage, Alaska. They show that traveling from Anchorage to Hong Kong, L varies from about 1 to 4, and for the Melbourne flight, L varies from about 1 to 2.25.

The bar chart in Figure 9 indicates that the measured total doses for all eight flights are within reasonable agreement with the predicted values obtained from the FAA model. The differences in those doses are due to the conversion from silicon doses to tissue doses and also due to the use of quality factors to obtain μ Sv. A factor of 1.2 for protons [23] will convert μ Gy(Si) to μ Gy(tissue). But, the quality factors needed to convert the latter to μ Sv depend on the primary particle type and energy incident on the detector for each of the eight flight paths evaluated in Figure 9. That is, the quality factors used in the FAA model would have to be applied to the data in Figure 9 to allow a direct numerical comparison to be made. Consequently, only effective quality factors based on the ratio of predicted to measured values can be calculated and they are shown in the figure.

In this context, it should be noted that comparisons with compatible results from other sources do not have to agree, even for identical departure and destination points, without either measurements being wrong. This may simply be due to instrument related causes, unit conversions, and/or to flight-path variations. While scheduled airlines are supposed to follow established flight corridors and altitudes, many times changes in course are made while on the way because of comfort, safety, traffic, or weather conditions. Therefore, preliminary flight plans issued before the actual departure are of no help in correctly analyzing and interpreting the measurements, especially in terms of magnetic latitude and altitude or environment conditions. For this purpose, a "corrected" flight plan is required which indicates for every course change the exact location (geographic coordinates), altitude, and "zulu" time, with several additional interim positional "fixes". This type of information was not available for the initial commercial flights reported in reference [7] but is now routinely being obtained for later analysis investigating long-term effects.

As stated before, the final objective of this research is to produce global maps of doses and fluxes reflecting the dynamic nature of the atmospheric radiation field. An example is the summary Table 2 which indicates the altitude and magnetic latitude dependence for quiet solar maximum conditions. It is obvious that a statistically significant base of data needs to be generated and analyzed with techniques being specifically developed for this work, not only in order to complete this table, but also in order to generate similar ones for other environment conditions, thereby addressing the study parameters listed in the "Background" section of this paper. In addition, a standard for comparison needs to be established by which local magnetospheric cutoff values and variations in local rigidity due to space weather, solar cycle, solar events, and magnetic storms can be evaluated. For example, significant diurnal variations occur in cutoff latitudes associated with geomagnetic tail effects (2-4 degrees) and with storm induced changes (>4 degrees).

XI. CONCLUSIONS

It has been shown from these aircraft measurements that the LoLRS is a suitable instrument that can be used to generate the large data base which is needed for a global mapping of doses, dose rates, and particle LET spectra at aviation altitudes over a time period that should include at least one solar cycle. Such extensive coverage would allow the dynamic nature and variability of the atmospheric radiation field to be qualitatively determined and would facilitate the construction of an initial empirical model or a substantial improvement of existing models. Dependencies of the data on temporal and spatial variations must be systematically included in the study of atmospheric cosmic-ray progeny and their effects. High-altitude, long-duration balloon measurements over the polar regions, where field lines are open to interplanetary space, are ideal to establish a standard for comparison to measurements at other locations on the globe, for a true definition of rigidity and magnetospheric attenuation. From the data analyzed so far in this initial phase of the study, the basic tenet of cosmic ray penetration and, hence, progeny distribution, is clearly evident: doses increase towards higher altitudes and for greater L-shell values (or equivalently: higher magnetic latitudes). Clearly, accurate global mapping of radiation dose and dose rates requires a wide range of measurements over long intervals of time because solar cycle, solar events, and space weather will also influence the results. Previous studies have identified some of the processes involved in the generation of cosmic ray secondaries, but none has related their intensities and distribution to environmental conditions.

XII. ACKNOWLEDGMENT

The authors wish to acknowledge the considerable and valuable contributions of Evergreen Airlines with special thanks to L. K. Lane, President, S. W. Leonard, Director of Operations, Corp. Headquarters, K. J. Rickard, Director of

Maintenance at JFK, and K. P. McGuire, Director of Airport Operations at JFK, which made it possible to collect data for this paper and also for their continuing support of the project.

[23] ICRP 1990, "Recommendation of the International Commission on Radiological Protection", Report 60, (Oxford Pergamon Press) 1991.

XIII. REFERENCES

- [1] Courtesy International Business Machines Corporation. Reprinted with permission of the IBM Journal of Research and Development, Vol. 40, No. 1, 1996.
- [2] A. Taber and E. Normand, "Single Event Upset in Avionics", *IEEE Trans. on Nucl. Sci.*, vol. 40, no. 2, pp. xxx, April 1993.
- [3] E. Normand and T. J. Baker, "Altitude and Latitude Variations in Avionics SEU and Atmospheric Neutron Flux", *IEEE Trans on Nucl. Sci.*, Vol. 40 No. 6, December 1993.
- [4] J. Olsen, P. E. Becher, P. B. Fynbo, P. Raaby, and J. Schultz, "Neutron-Induced Single Event Upsets in Static RAMS Observed at 10 KM Flight Altitude", *IEEE Trans on Nucl. Sci.*, Vol. 40, No. 2, April 1993.
- [5] E. Normand, "Single-Event Effects in Avionics", *IEEE Trans. on Nucl. Sci.*, Vol. 43, No. 2, April 1996.
- [6] E.G. Stassinopoulos, C.A. Stauffer, and G.J. Brucker, "Miniature High-LET Radiation Spectrometer for Space and Avionics Application", *Nucl. Instr. & Methods in Phys. Res., Section A*, A 416, 1996.
- [7] E.G. Stassinopoulos, C.A. Stauffer, T.P. Dachev, G.J. Brucker, B.T. Tomov, and P.G. Dimitrov, "The LFULIN-3M Radiometer for Measuring Particle Doses in Space and on Aircraft", NASA/TM-2002-210003, February 2002.
- [8] C. S. Dyer, A. J. Sims, J. Farren, and J. Stephen, "Measurements of the SEU Environment in the Upper Atmosphere", *IEEE Trans. on Nucl. Sci.*, Vol. 36, No. 6, December 1989.
- [9] C. S. Dyer, A. J. Sims, J. Farren, J. Stephen, "Measurements of Solar Flare Enhancements To the Single Event Upset Environment in the Upper Atmosphere", *IEEE Trans. on Nucl. Sci.*, Vol. 37, No. 6, December 1990.
- [10] M. Furukawa, S. Zhang, S. Zhao, Z. Jiang, L. Nei, W. Chung, M. Matsumoto, and S. Tokonami, "Variation of Cosmic-ray Intensity with Altitude in Asia: Results for Japan, China, and Korea", National Institute Of Radiological Sciences, Annual Report, April 1998-March 1999.
- [11] R. Beaujean, J. Kopp and G. Reitz, "Radiation Exposure In Civil Aircraft", *Radiation Protection Dosimetry*, Vol. 85, Nos. 1-4, 1999.
- [12] T. Nakamura, y. Uwamino, T. Ohkubo, and A. Hara, "Altitude Variation Of Cosmic-Ray Neutrons", *Health Physics*, Vol. 53, No. 5, November 1987.
- [13] C. E. Meilwain, "Coordinates for Mapping the Distribution of Magnetically Trapped Particles", *J. Geophys. Res.*, 66, 3681, 1961
- [14] D. F. Smart and M. A. Shea, "The Distribution of Galactic Cosmic Rays and Solar Particles to Aircraft Altitudes". *Proceedings for the Topical Meeting on New Horizons in Radiation Protection and Shielding*, American Nuclear Society, 1992.
- [15] E. Normand and T. J. Baker, "Altitude and Latitude Variations in Avionics SEU and Atmospheric Neutron Flux" *IEEE Trans. on Nucl. Sci.*, Vol. 40, No.6, December 1993.
- [16] E.G. Stassinopoulos, "Radiation Environments of Space", *IEEE International Radiation Effects Conference, Short Course on Microelectronics for the Natural Radiation Environment of Space*, Reno, NV, July 16, 1990.
- [17] A. Taber and E. Normand, "Single Events in Avionics", *IEEE Trans. Nucl. Sci.*, Vol. 40, No. 2, April 1993.
- [18] R.B. Mendall and S.A. Korff, "Fast Neutron Flux in the Atmosphere", *J. Geophys. Res.*, 68, 5487, 1993.
- [19] S.S. Holt et al., "Fast Neutron Latitude Variations in the Atmosphere at Solar Minimum", *J. Geophys. Res.*, Vol. 71, p. 5109, 1966.
- [20] J. Hewitt et al., "AMES Collaborative Study of Cosmic Ray Neutrons: Mid-Latitude Flights", *Health Physics*, 34, 375, 1978.
- [21] J.W. Wilson and J.E. Nealy, "Model and Data Base for Background Radiation Exposure of High Altitude Aircraft", *Proceedings of the Topical Meeting on New Horizons in Radiation Protection and Shielding*, American Nuclear Society, 1992.
- [22] A.N. Tsyganenko and D.P. Stern, "Modeling the Global Magnetic Field of the Large-Scale Birkeland Current System", *J. Geophys. Res.*, 101, pp. 27187-27198, 1996.